Received: 26 January 2021 | Revised: 24 June 2021 | Accepted: 29 July 2021

DOI: 10.1002/jbm.a.37293

ORIGINAL ARTICLE

Society For Biomaterials | WILEY

Semiautomated quantification of the fibrous tissue response to complex three-dimensional filamentous scaffolds using digital image analysis

Friedrich Barsch[1,2] | Andreas Mamilos[2] | Maximilian Babel[2,3] | Willi L. Wagner[4,5] | Hinrich B. Winther[6] | Volker H. Schmitt[7] | Helmut Hierlemann[8] | Andreas Teufel[9] | Christoph Brochhausen[2,3]

[1]Institute for Exercise and Occupational Medicine, Faculty of Medicine, Medical Center, University of Freiburg, Freiburg, Germany

[2]Institute of Pathology, University Regensburg, Regensburg, Germany

[3]Central Biobank Regensburg, University Regensburg and University Hospital Regensburg, Regensburg, Germany

[4]Department of Diagnostic and Interventional Radiology, University Hospital Heidelberg, Heidelberg, Germany

[5]Translational Lung Research Centre Heidelberg (TLRC), German Lung Research Centre (DZL), Heidelberg, Germany

[6]Institute for Diagnostic and Interventional Radiology, Hannover Medical School, Hannover, Germany

[7]Department of Cardiology, Cardiology I, University Medical Center Mainz, Johannes Gutenberg-University of Mainz, Mainz, Germany

[8]PolyMedics Innovations GmbH, Denkendorf, Germany

[9]Department of Medicine II, University Medical Center Mannheim, Medical Faculty Mannheim, Heidelberg University, Mannheim, Germany

Correspondence
Christoph Brochhausen, Institute of Pathology, University Regensburg and Central Biobank Regensburg, University Regensburg and University Hospital Regensburg, Franz-Josef-Strauß Allee 11, Regensburg 93053, Germany.
Email: christoph.brochhausen@klinik.uni-regensburg.de

Abstract

Fibrosis represents a relevant response to the implantation of biomaterials, which occurs not only at the tissue–material interface (fibrotic encapsulation) but also within the void fraction of complex three-dimensional (3D) biomaterial constructions (fibrotic ingrowth). Usual evaluation of the biocompatibility mostly depicts fibrosis at the interface of the biomaterial using semiquantitative scores. Here, the relations between encapsulation and infiltrating fibrotic growth are poorly represented. Virtual pathology and digital image analysis provide new strategies to assess fibrosis in a more differentiated way. In this study, we adopted a method previously used to quantify fibrosis in visceral organs to the quantification of fibrosis to 3D biomaterials. In a proof-of-concept study, we transferred the "Collagen Proportionate Area" (CPA) analysis from hepatology to the field of biomaterials. As one task of an experimental animal study, we used CPA analysis to quantify the fibrotic ingrowth into a filamentous scaffold after subcutaneous implantation. We were able to demonstrate that the application of the CPA analysis is well suited as an additional fibrosis evaluation strategy for new biomaterial constructions. The CPA method can contribute to a better understanding of the fibrotic interactions between 3D scaffolds and the host tissue responses.

KEYWORDS
biocompatibility, biomaterial, fibrosis, semiautomatic scoring

1 | INTRODUCTION

The pathogenesis of fibrosis plays not only a critical role in the tissue response to acute or chronic organ damage, it is also important in the field of tissue engineering (TE) and regenerative medicine. In this context, fibrosis represents one part of the foreign body reaction to biomaterials.[1,2] The implantation of synthetic biomaterials induces a multistep tissue response: the primary injury, caused by the implantation of a biomaterial, is followed by an inflammatory reaction, which finally leads to a fibrotic encapsulation of the implants.[1-3] Here, the cellular, biochemical, and pathophysiological aspects of the fibrous tissue response are complex and still not fully understood. Specifically in the context of macroporous 3D biomaterial scaffolds, the fibrotic reaction manifests not only on the surface around the entire scaffold but also in the void space between the structural elements of the scaffold. Recent technical developments in histopathological analytics provide valuable tools for the morphometric analysis on digitalized microscopic images. Digital slide scanners are routinely used and working processes are widely accelerated and automated. The digitalization of histopathological slides provides a range of new computerized evaluation strategies for a quantitative analysis of fibrotic reactions. Also, the histopathological evaluation of biomaterial-induced fibrosis may benefit from this development. Tissue-engineered products underlie continuous development. However, these developments are in discrepancy to the development of appropriate evaluation tools.[4,5]

1.1 | Evaluation strategies for biomaterial induced fibrosis

Until today, one of the most established methods for the histopathological evaluation of soft tissue reactions on implants is represented by the international standard ISO 10993-6, an instrument that should be understood as a continuously evolving document.[4] This standard determines evaluation procedures based on semiquantitative and quantitative ratings. A semiquantitative scoring system classifies the fibrous tissue response on a subcutaneously implanted biomaterial in five categories (0, narrow band, moderately thick band, thick band, and extensive band), while the rare quantitative rating systems of fibrotic reactions are only based on the thickness of the fibrous capsule around the implants.[6] But the fibrotic reaction on macroporous matrices, like decellularized grafts, freeze-dried scaffolds, microfiber meshes or 3D-printed scaffolds, which are in use for cartilage and skin TE, is not only characterized by an encapsulation at the implants surface but also by the fibrotic ingrowth dependent of their complex 3D geometry.[7-9] During the implantation period, fibrogenic effector cells migrate into the pores of 3D scaffolds and produce ECM proteins in the void space of the biomaterial structural elements. This infiltrating fibrotic growth is not adequately represented by the commonly used analytical tools. Still semiquantitative assessments remain in use to measure this fibrous tissue response on biomaterials.[10-18] Although practical to use, these methods show significant disadvantages: they are in a way unspecific, subjective, lab-to-lab variable and not uniformly applicable to the diversity of existing biomaterial designs.[4,5,19] It turns out that these biocompatibility assessments cannot account for the rapidly growing variety of different tissue-engineered scaffold designs. Important morphometric information about fibrotic shapes in relation to the scaffold designs is not accounted for. The development of the histopathological evaluation methods is lagging behind the development of scaffold designs.[4,5] Hence, several authors demand for more sophisticated quantitative histopathological evaluation strategies and biological tests.[4,5,19,20] For example, in 2016, Anderson et al. criticized that quantitative assays and statistical analysis are rarely addressed in the fields of TE and regenerative medicine. They called for new strategies to identify and specify tissue responses to tissue-engineered scaffolds.[4] Around the millennium, several experimental studies in hepatology dealt with the comparison of semiquantitative scores and quantitative digital image analysis (DIA).[21-30] As a result, one of the most established methods to quantify liver fibrosis today is the analysis of the "Collagen Proportionate Area" (CPA) in digitalized micrographs of the liver specimens.[28-39] As the term reveals, this ratio describes the area proportion of collagen fibrils in a defined image area. The collagen content is representative for the extent of fibrosis.

1.2 | Aims and purposes of the study

The aim of the present proof-of-concept study was to assess the suitability of CPA analysis for the quantitative evaluation of the fibrotic ingrowth in the void space of structural elements of complex 3D scaffold-based biomaterials subcutaneously implanted in pigs. In addition, we wanted to analyze the encapsulation of the scaffolds with DIA and compare both DIA methods with corresponding semiquantitative methods. With the present study, we want to contribute to the development of new histopathological assessment strategies for novel complex biomaterial designs. We present a new approach to assess scaffold-induced fibrosis in a quantitative, semiautomatic manner. Furthermore, we give a detailed description of the applied method to make it transparent, comprehensible, repeatable, and reliable.

2 | MATERIALS AND METHODS

2.1 | Study design and biomaterial scaffolds

The histopathologic analyses were performed with explants from an experimental animal study to evaluate different scaffold materials. The animal experiment was authorized under the reference number V3-2347-A-6-19-2013 in accordance with the European Guideline Directive 90/385/EEC and the German provisions of the Animal Welfare Act. In this study, four pigs were used to analyze novel synthetic biomaterial scaffolds with respect to their soft tissue reactions. The scaffolds were developed and provided by Polymedics (Polymedics GmbH, Denkendorf, Germany). Geometrically, the scaffolds are

composed of smooth filaments that form a complex randomly organized 3D macroporous network. In total, 16 filamentous scaffolds were created and alphabetically named (scaffold A-P). In preparation of their subcutaneous implantation, skin areas (=test fields) were defined for each animal from cranial to caudal, bilateral, and paravertebral on their dorsal sites. The test fields measured 4×4 cm^2. The animals were premedicated with an intramuscular injection of 15 mg/kg ketamine, 0.25 mg/kg midazolam, and 0.4 mg/kg azaperone. Then the animals were intubated and connected to a mechanical ventilator. Vital signs were controlled with continuous ECG- and SpO_2-monitoring. Under proper anesthesia with a continuous infusion of ketamine (10 mg/kg/h) and midazolam (0.5 mg/kg/h) via peripheral vein, the animals received an operation procedure in which subcutaneous pockets with a skin flap were prepared with scalpel, scissors, and tweezers. The filamentous fleeces ($N = 16$) were distributed and inserted into the subcutaneous implantation pockets (one fleece per pocket). After implantation of the biomaterial, the subcutaneous pockets were covered and sutured with the skin flaps. Afterwards, the test fields were bandaged. During the observation period, the animals received frequent dressing changes. On postoperative day 25, the biomaterial scaffolds were completely excised with an edge seam of surrounding skin tissue. The explants were immediately fixed in 4% buffered formalin solution.

2.2 | Sample preparation and histological staining

The explants of the animal experimental study were liberated from bristles. Specimens were taken for histopathological analyses: one from the center (Slide 1) and the other 10 mm peripheral from the center of the skin fields (Slide 2). The samples were transferred into embedding cassettes (Kabe Labortechnik GmbH, Nümbrecht-Elsenroth, Germany), dehydrated, and embedded in paraffin in a fully automated manner using a Tissue-Tek® VIP™ processor (SAKURA® Finetek Germany GmbH, Staufen, Germany). Thereafter, the resulted paraffin blocs were cooled (QUICK COOL UNIT - TKF 22, MEDITE GmbH, Burgdorf, Germany) and cut with the rotary microtome HYDRAX M55 (Carl Zeiss Microimaging GmbH, Jena, Germany) in 4-µm-thick sections. The sections were placed on glass slides (Diagonal GmbH & Co. KG, Münster, Germany), dried, and deparaffinized for 20 min at 61° with a heat device (Heraeus Function Line B6, Thermo Scientific Heraeus Function Line UB6, Thermo Scientific Heraeus Function Line B 6060, Thermo Fisher Scientific GmbH, Dreieich, Germany). In preparation for the staining procedure, the sections were immersed for 3×5 min in Xylol (SAV Liquid Production GmbH, Flintsbach am Inn, Germany) to wash out paraffin remnants, followed by rehydration in graded alcohol (SAV Liquid Production GmbH, Flintsbach am Inn, Germany), and finally washed with distilled water. Sections were stained with Masson–Goldner's trichrome staining, to differentiate collagen fibers from the surrounding tissue. Masson–Goldner's trichrome staining is widely used for the analysis of fibrosis in organs and for the evaluation of the fibrotic response to biomaterials.[14,35,38,40-47] As a result of this procedure, collagen fibers appear in a bright green color in bright field light microscopy, which produces excellent contrast for analysis with digital image quantification. Afterwards, the slides were processed to permanent histological slides with Entellan (VWR International GmbH, Darmstadt, Germany) in a Leica CV5030 fully automated glass coverslipper (Leica Microsystems GmbH, Wetzlar, Germany). Thus, in total 32 slides ($N = 32$) were created and analyzed.

2.3 | Slide digitalization and ROI definition

In accordance with modern digital pathology strategies, we based the DIA on whole slide imaging.[48] Therefore, all 32 Masson–Goldner's trichrome-stained slides were digitized in one automated run with a digital slide scanner (NanoZoomer 2.0 HT, Hamamatsu Photonics Deutschland GmbH, Ammersee, Germany). The scanning process was accomplished with the following settings: scanning method: time delay integration; scanning resolution: 20×. These settings resulted in high-quality image file (.ndpi-format) with a resolution of 456 nm per pixel. The scans were examined with the compatible image viewing software NDP.view 2 (Hamamatsu Photonics Deutschland GmbH, Ammersee, Germany) regarding their image quality and scanning artifacts, which could influence the performance of our DIA. With an overall orientation, we identified the typical histological stratification and subdivisions of cutis and subcutis. All slides showed the structural elements of the biomaterial scaffolds in the subcutaneous zone. This biomaterial area was set as region of interest (ROI). Particularities, like cutting artifacts, were excluded from the ROI. The "Export Image" function of the NDP.view 2 software allows to create images in different magnifications.

2.4 | Semiquantitative histopathological analysis

Semiquantitative analysis was performed by a trained investigator with the help and supervision of an experienced pathologist. The image sequences and the digitized slides that were also used for the DIA served as the basis for the semiquantitative grading. The investigator was trained with the help of some sample images and was asked to examine the following parameters: (a) fibrotic encapsulation around the whole scaffold and (b) fibrotic ingrowth in between the structural elements of the scaffold. The examiner categorized the fibrotic encapsulation and the fibrotic ingrowth according to the common histopathological scoring assessments.[5,49] In this context, the encapsulation has been graded according to an ordinal scale as follows: (0) no fibrous encapsulation, (1) minimal encapsulation, (2) mild encapsulation, (3) moderate encapsulation, and (4) extensive encapsulation. The fibrotic ingrowth was also classified according to an ordinal scale: (0) absent, (1) minimal, narrow band, 1–2 cell layers thick, (2) thin, localized band, <10 cell layers thick, (3) moderately thick, contiguous band along the length of tissue, (4) extensive, thick zone with effacement of local architecture.

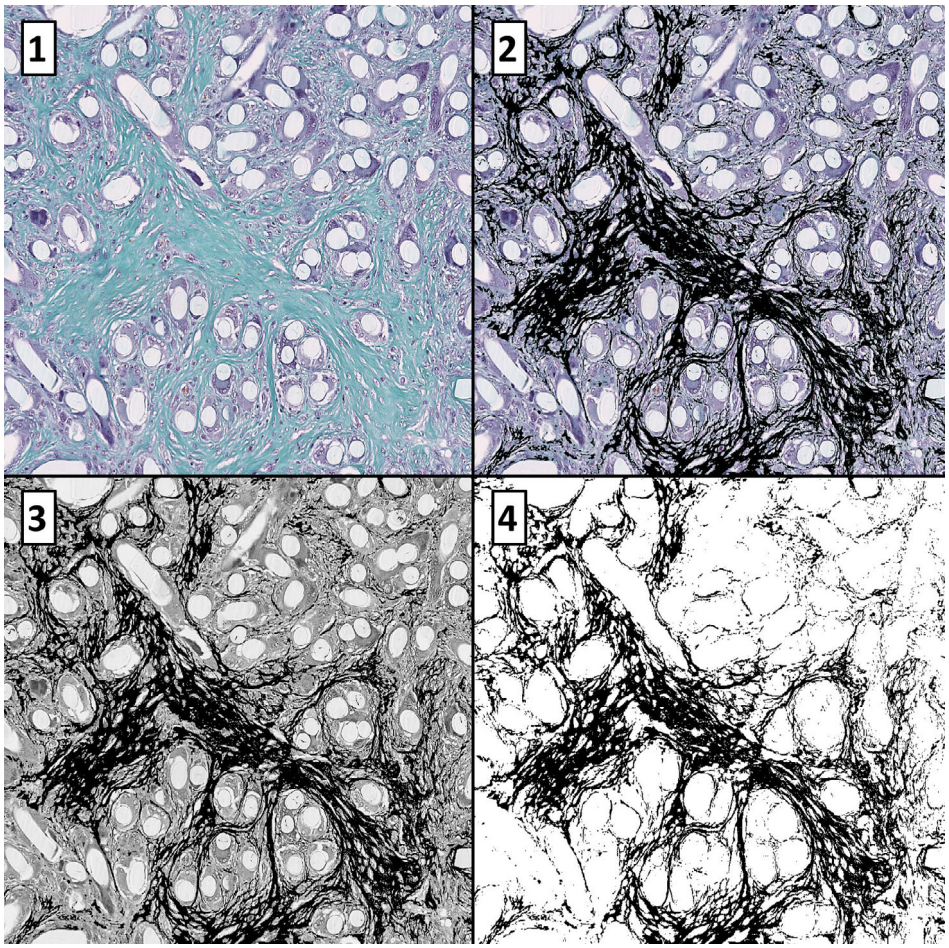

FIGURE 1 The image sequence shows the single steps of image processing of the collagen proportionate area (CPA) method for the detection and segmentation of the fibrotic ingrowth. (1) Original histologic image in Masson–Goldner's trichrome staining, 100-fold magnification. Recognize the filaments of the biomaterial scaffold and the collagen fibers, which appear in bright green. (2) The "Color Threshold" function allows to depict the collagen fibers and marks them black. (3) After conversion to an 8-bit version, the image appears in grayscale. (4) The threshold function allows for binarization of the image. The CPA previously marked in black pixels can be calculated. Thus, CPA values describe the percentage of the area of collagen fibers in the total area of an image

2.5 | Quantitative histopathological analysis with DIA

2.5.1 | CPA analysis

We performed computer-assisted, semiautomatic CPA analysis with the open-source image analysis software, ImageJ (version 1.49, National Institutes of Health), which is widely used for fibrosis quantification and, as a public domain, it is widely accessible.[30,50-53] In each slide, 10 images in 100× magnification were randomly selected from the ROI and exported as .jpeg data. Each image had a sample area of 0.866 mm^2 with a resolution of 1368 × 768 pixels. The images (320 in total) form the basis of the CPA analysis. ImageJ provides a function to process several images at once. Thus, we could import all images of each slide as a series ($N = 10$) with the "File - Import - Image sequence" path. Then, we used the "Color threshold" function to mark the green-stained collagen fibers in the images. Regarding this, we used the following settings: Thresholding method: "Default," Threshold color: "Black," Color space: "HSB." The parameters "Hue," "Saturation," and "Brightness" were adjusted for each image sequence to capture only the collagenous fibers that appeared in bright green. The "stack"-bottom allowed to employ the settings on all imported images. Subsequently, the images were converted into 8-bit images. Next, we used the "Threshold" function of the software with the following settings: "Default," "B&W," (black and white) and set both scale bars to zero. As a result, binarized black and white images were created, in which the previously marked collagen fibers remain black and the background is set to white (Figure 1). To optimize the detection of the collagen fibers, all black and white images were compared with the original colored images. If necessary, manual corrections were performed, using the white "Pencil" tool to eliminate incorrect segmentations. Afterwards, the settings for measurement were defined. The "Area" and the "Area fraction" of each converted image were calculated, yielding the collagen area fraction based on the number of black pixels in relation to the total amount of pixels in each image. Thus, CPA values represent the area fraction of collagenous fibers in the total area of an image. CPA values of all processed images are provided as percentages in a results table and can easily be exported for further statistical analysis. The quantitative character of CPA values is defined by a metric scale on a rational-scale level with a range from 0% to 100%.

2.5.2 | Fibrous capsule thickness measurements

We used NDP.view 2 software (Hamamatsu Photonics Deutschland GmbH, Ammersee, Germany) to determine the thickness of the fibrous capsule around the scaffolds. The software provides a ruler

tool, which allows us to measure distances in μm. We defined 10 measure points for each slide—5 points superficial and 5 points underneath the biomaterial. At each point, we measured the distance of the collagen layers between the scaffold and the surrounding subcutaneous fat cells. The measurements were performed perpendicular to the long axis through the scaffold. To find the exact boundary layers between the scaffold and the fibrous capsule, as well as the fibrous capsule and the subcutaneous fat cells, we managed this process in 200-fold magnification (Figure 2). Statistically, the quantitative character of fibrous capsule thickness (FCT) values is defined by a metric scale on a rational-scale level with a range from 0 μm to infinite μm.

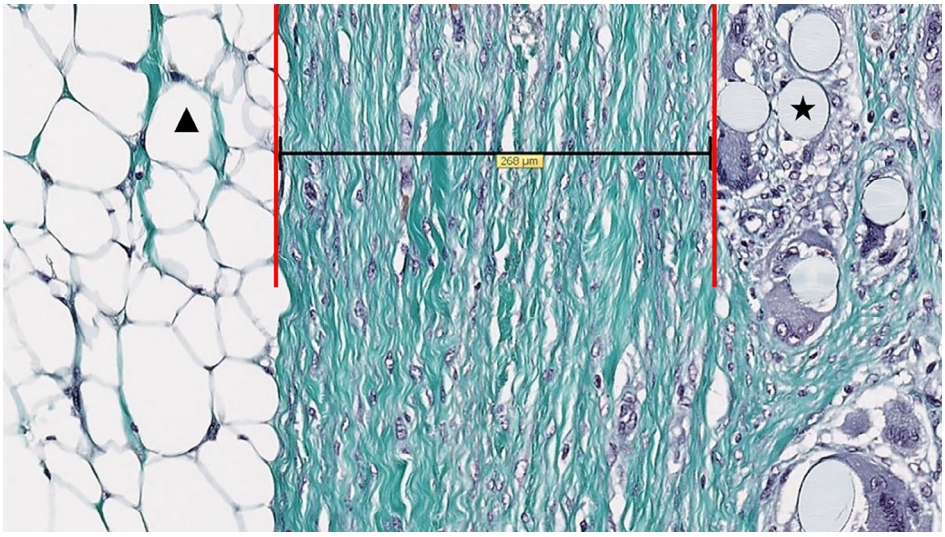

FIGURE 2 Measurement procedure of fibrous capsule thickness (delineated by red lines). The triangle marks the subcutaneous fat cells (black triangle) that form the outer border of the capsule. Note the parallel orientation of the collagenous fibers around the surface of the biomaterial filaments (black star) in contrast to the tortuous course of the collagenous fibers within the void space of the scaffold. Masson–Goldner's trichrome staining, 200-fold magnification

TABLE 1 Results of the quantitative and semiquantitative evaluations of the fibrotic ingrowth in the void space on macroporous filamentous biomaterial scaffolds

Fibrotic ingrowth				
	Slide 1		Slide 2	
Scaffold ID	Quantitative analysis CPA (%)	Semiquantitative score	Quantitative analysis CPA (%)	Semiquantitative score
A	29.65 (25.25 – 33.14)	2	19.18 (17.08 – 22.96)	2
B	16.70 (14.39 – 25.28)	3	8.75 (3.70 – 14.02)	2
C	16.67 (8.37 – 22.82)	3	32.05 (22.99 – 38.88)	2
D	32.20 (17.38 – 50.33)	3	13.65 (10.93 – 21.45)	2
E	29.92 (21.51 – 42.46)	4	22.94 (14.44 – 32.58)	4
F	17.53 (13.43 – 18.97)	3	20.31 (15.95 – 23.11)	2
G	13.00 (10.13 – 18.32)	2	22.00 (10.28 – 27.53)	3
H	14.39 (8.86 – 18.93)	2	11.97 (10.62 – 16.40)	2
I	11.98 (7.25 – 29.00)	2	20.53 (14.18 – 24.41)	2
J	11.02 (5.70 – 19.22)	2	7.56 (4.52 – 9.00)	2
K	12.12 (5.79 – 21.94)	2	11.05 (7.64 – 18.75)	2
L	27.61 (19.74 – 49.41)	3	20.05 (13.94 – 30.92)	3
M	15.22 (12.75 – 25.43)	2	14.27 (11.24 – 18.66)	2
N	19.08 (12.59 – 20.64)	2	9.84 (7.81 – 13.48)	2
O	18.82 (8.98 – 25.99)	4	27.85 (18.01 – 46.14)	4
P	8.37 (4.26 – 13.47)	2	8.49 (4.95 – 18.56)	2

Note: CPA values represent the area fraction of collagenous fibers (in %) in a defined total area of an image from the ROI. The CPA measurements of 10 images were included in each CPA data set. The data are metrically scaled on a rational scale level from 0% to 100%. The values are presented as medians and interquartile ranges for each slide according the corresponding scaffold. The corresponding semiquantitative ratings of the fibrotic ingrowth of the scaffolds are categorized at an ordinal scale level: (0) absent fibrosis, (1) minimal, narrow band, 1–2 cell layers thick, (2) thin, localized band, <10 cell layers thick, (3) moderately thick, contiguous band along length of tissue, and (4) extensive, thick zone with effacement of local architecture.

TABLE 2 Results of the quantitative and semiquantitative evaluations of the fibrotic encapsulation around macroporous filamentous biomaterial scaffolds

Fibrotic encapsulation				
Slide group 1			**Slide group 2**	
Scaffold ID	Quantitative analysis FCT (μm)	Semiquantitative score	Quantitative analysis FCT (μm)	Semiquantitative score
A	172.00 (74.98 – 233.25)	2	27.50 (24.40 – 52.33)	1
B	121.50 (41.85 – 213.25)	3	80.70 (25.98 – 180.75)	2
C	47.50 (24.43 – 107.55)	2	119.50 (62.70 – 183.75)	2
D	180.00 (106.38 – 249.50)	3	75.00 (25.48 – 111.43)	2
E	1460.00 (626.25 – 1860.00)	4	571.50 (279.25 – 755.00)	4
F	121.50 (66.03 – 155.00)	3	152.00 (91.43 – 267.50)	3
G	83.40 (48.63 – 121.68)	3	241.50 (50.08 – 377.25)	3
H	81.50 (56.50 – 150.75)	2	29.05 (22.50 – 80.88)	1
I	100.95 (64.65 – 203.25)	4	89.20 (31.55 – 271.00)	2
J	123.00 (57.48 – 167.00)	3	137.50 (44.25 – 357.75)	2
K	72.80 (42.33 – 130.48)	2	230.00 (127.18 – 640.25)	3
L	214.80 (148.65 – 603.25)	4	224.50 (40.70 – 411.25)	3
M	187.50 (85.40 – 298.25)	3	126.50 (74.98 – 188.00)	2
N	168.50 (92.40 – 340.50)	3	194.50 (84.88 – 333.00)	2
O	124.05 (74.68 – 452.75)	4	487.00 (64.53 – 1100.00)	4
P	68.90 (50.68 – 187.00)	3	89.00 (32.35 – 439.25)	3

Note: Fibrous capsule thickness (FCT) values represent the thickness of the fibrous capsule (in μm), which was measured at 10 locations around each scaffold with a digital ruler tool provided by the slidescanner software. The data are metrically scaled on a rational scale level from 0 μm to infinite μm. The values are presented as medians and interquartile ranges for each slide according the corresponding scaffold. The corresponding semiquantitative ratings are categorized at an ordinal scale level: (0) no fibrous encapsulation, (1) minimal encapsulation, (2) mild encapsulation, (3) moderate encapsulation, and (4) extensive encapsulation.

2.6 | Statistical analysis

Statistical analysis was performed using the statistical software IBM SPSS Statistics (version 25.0, IBM Deutschland GmbH, Ehningen, Germany). Regarding the animal study design and the histological processing, 32 slides ($N = 32$) were created and 10 CPA and 10 FCT values were collected per slide. The data sets for each quantitative fibrosis evaluation method (CPA and FCT) were examined regarding their distribution with one-sample Kolmogorov–Smirnov test with significance levels of $p < .05$. Here, the asymptotic significance (2-sided) was Lillifors corrected. Because most data sets possessed skewness of the data distribution, the results are presented as medians and interquartile ranges. The biomaterial scaffolds (A-P) were compared according to the slide group using the independent-samples Kruskal–Wallis test with a significance level of $p < .05$. Furthermore, bivariate correlations were performed between the slide-specific median values of CPA, FCT, and the corresponding semiquantitative scores using Spearman's rank coefficient with significance levels of $p < .01$.

3 | RESULTS

During the subcutaneous implantation period, all scaffolds induced a fibrotic host response. Histologically, this reaction was characterized by the formation of a fibrous capsule around the implants surface in to and by a fibrotic growth into the void space of the macroporous scaffold structure. The fibrotic capsule was formed by multiple collagen layers with parallel orientation around the surface of the whole scaffold. In contrast to the fibrous encapsulation, the organization of collagen bundles within the void space of the filament scaffold, representing the fibrotic ingrowth, was complex with a tortuous and convolved architecture in between the filaments of the scaffolds (Figure 1). Under qualitative aspects, all prepared slides were suitable for DIA. CPA values were measured for the fibrotic ingrowth, as well as FCT values of the fibrotic encapsulation in each slide. The results of our applied methods for fibrosis evaluation are presented in tables and graphs in comparison between each slide of the 16 filamentous scaffolds (scaffolds A-P). Kolmogorov–Smirnov test revealed a left-leaning skewed data distribution with an asymptotic significance of $p < .001$ in most of our data sets (Lilliefors corrected). The semiquantitative histopathological scoring rated the fibrotic ingrowth of the scaffolds with values from minimum 2 to maximum 4 (Table 1). The semiquantitative evaluation of the encapsulation of the scaffolds revealed the values from minimum 1 to maximum 4 (Table 2).

Regarding the quantitative analyses, the median thickness of the fibrotic capsules and the median CPA values differed in between the scaffolds according to the slide group (Figures 3 and 4). In slide group 1, Kruskal–Wallis testing revealed an unequal data distribution

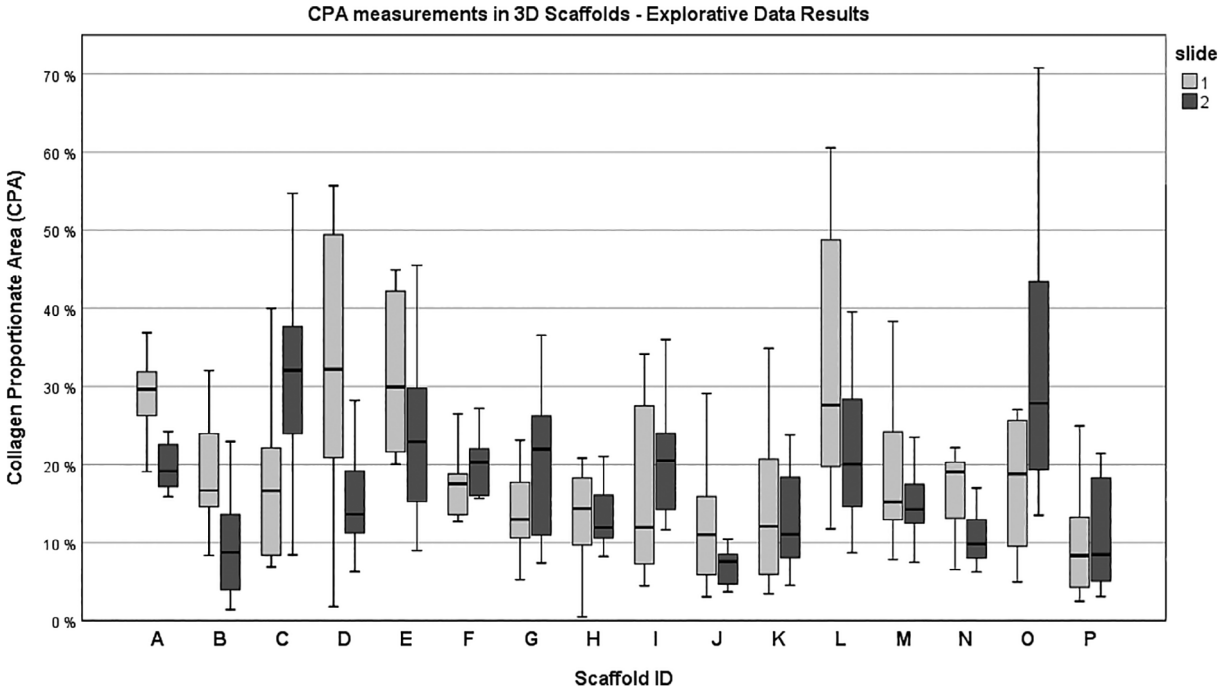

FIGURE 3 The box plot diagram presents the results of the quantitative data collection of the collagen proportionate area (CPA) measurements of each slide according to the scaffolds

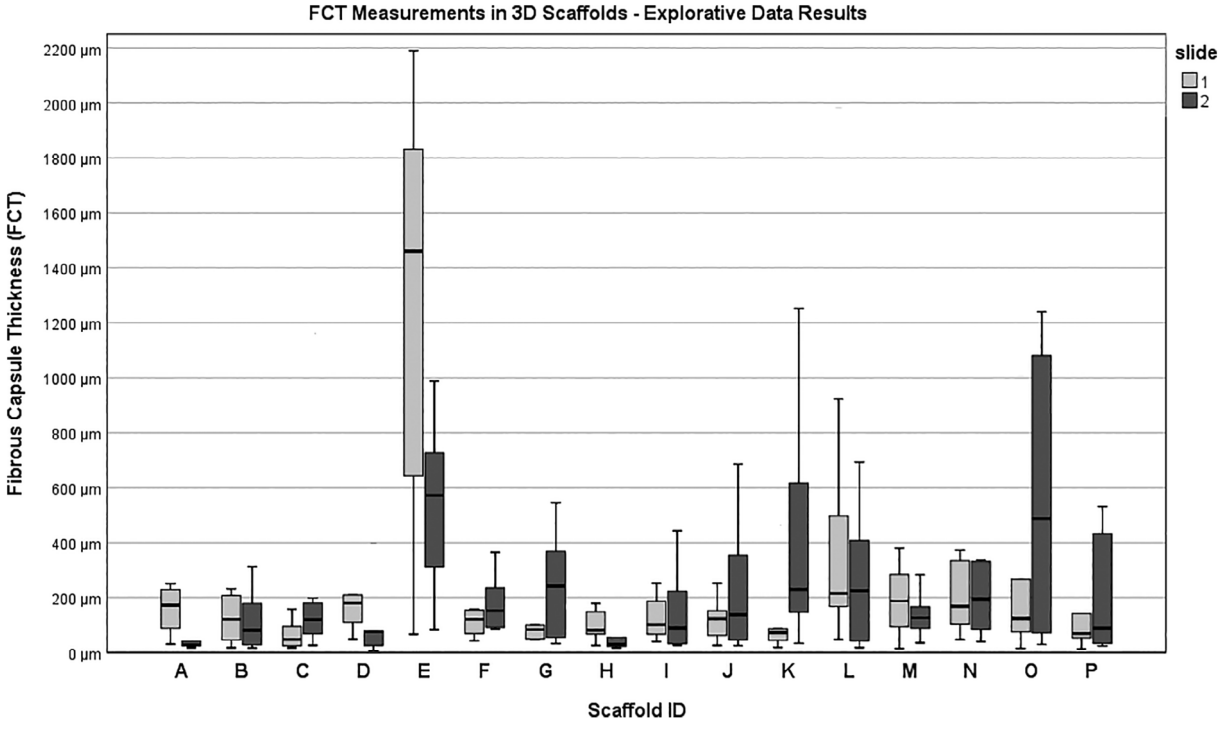

FIGURE 4 The box plot diagram presents the results of the quantitative data collection of the fibrous capsule thickness (FCT) measurements of each slide according to the scaffolds

of the CPA values across the scaffolds ($p < .001$). This also applies to slide group 2 ($p < .001$). The Kruskal–Wallis test also revealed that FCT data are unequally distributed across the scaffolds in both slide group 1 ($p < .001$) and slide group 2 ($p < .001$). The quantitative analyzation of median CPA values ranged between minimum 7.56% (Scaffold J, slide 2) to maximum 32.20% (Scaffold D, slide 1). Median FCT values ranged between minimum 27.50 µm (Scaffold A, slide 2) to maximum 1460.00 µm (Scaffold E, slide 1).

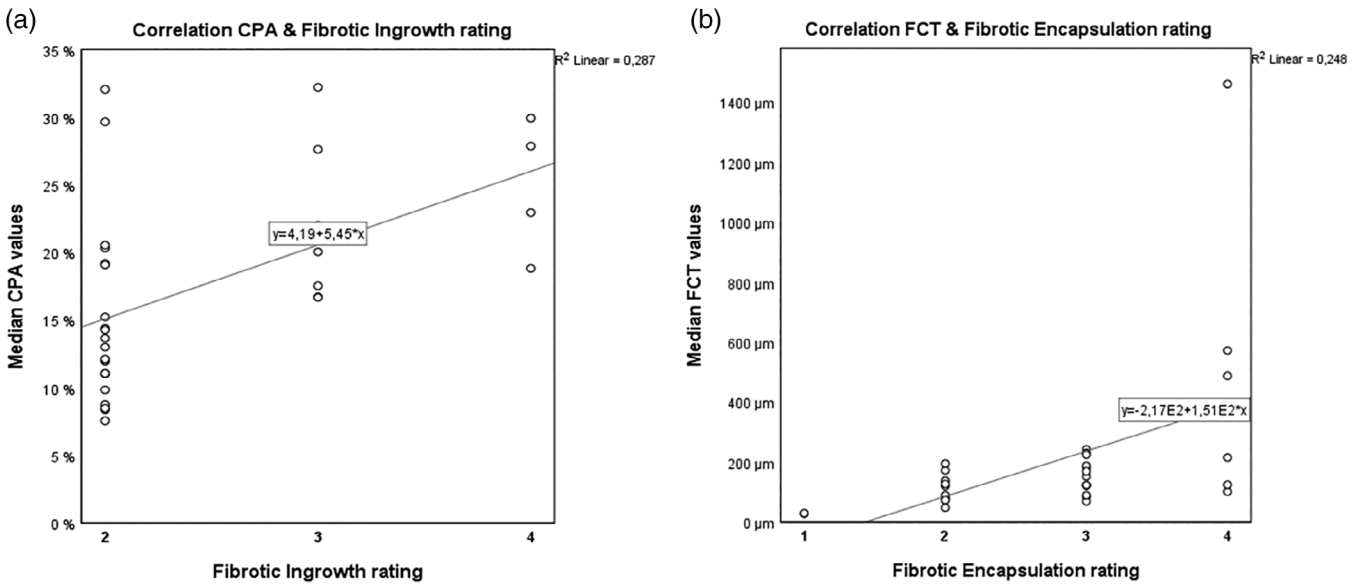

FIGURE 5 The scatter plots show the results of the bivariate correlations (Spearman) between (1) quantitative collagen proportionate area (CPA) measurements and semiquantitative fibrotic ingrowth ratings and (2) quantitative fibrous capsule thickness (FCT) measurements and semiquantitative fibrotic encapsulation ratings

The comparison of the semiquantitative analysis method with the quantitative DIA methods revealed significant bivariate correlations (Figure 5). Spearman's rank correlation between median CPA values and semiquantitative fibrotic ingrowth ratings of each slide detected the following results: CPA analysis correlated significantly with semiquantitative fibrotic ingrowth scores ($r = 0.568$, $p = .001$) at a significance level of $p < .01$ (two-tailed). Spearman's rank correlation between median FCT values and semiquantitative encapsulation ratings of the slides also detected a significant correlation ($r = 0.605$, $p < .001$) at a significance level of $p < .01$ (two-tailed).

4 | DISCUSSION

It is well known that physical and chemical characteristics of a biomaterial can influence the cell behavior and tissue responses of the foreign body reaction against biomaterials.[54-58] In TE research, great efforts have been made to take advantage of this and develop new biomaterials to achieve different goals, regarding their respective application fields. For example, in skin TE, one goal is to minimize the scar formation during wound healing.[59] Another aim for scaffold-based skin substitutes is to reach a good attachment and incorporation of the matrix to guarantee the repopulation of host cells and the replacement and remodeling of the ECM.[60] To check whether biomaterials reach the defined goals, semiquantitative histopathologic evaluation strategies are useful to examine the biomaterial-induced fibrosis. Unfortunately, a semiquantitative scoring system does not reflect very detailed and differentiated information about the biomaterial-induced fibrosis. Specifically in macroporous scaffolds, the fibrosis reaction presents itself in at least two different growth patterns. On the one hand, there is a fibrous encapsulation around the entire scaffold. On the other hand, there is a fibrotic ingrowth of collagen fibers into the scaffold interstices. In this context, the encapsulation and the fibrotic ingrowth may vary between different biomaterial designs. Moreover, slight changes of fibrotic extend during observation periods or small differences between biomaterials are not adequately reflected. Therefore, in preparation of histopathological analysis, we studied several quantitative evaluation methods for fibrosis in the literature. Although we found several references, that analyzed fibrotic reactions in different organs, quantitative assessments for biomaterial-induced fibrosis were very rare. Furthermore, the evidence on the histopathological quantification of the fibrous tissue response on 3D scaffold-based biomaterials is extremely insufficient. However, differentiated strategies for fibrosis evaluation for tissue-engineered scaffolds are demanded and necessary, especially because the variety of designs and their implementations are rising.[4,5,19,20] This proof-of-concept study demonstrates that DIA methods are helpful to obtain objective data on the fibrotic reaction to complex 3D biomaterial scaffold designs. As DIA methods are known to be powerful methods to quantify organ fibrosis, we applied CPA analysis, which is mainly known from liver cirrhosis research, to quantify the fibrotic ingrowth response on 3D synthetic biomaterial scaffolds.[28,53] Meanwhile, CPA analysis is often in use to evaluate fibrosis in several other organs. Subsequently, there are many processing differences among a multitude of CPA procedures. Unfortunately, in numerous descriptions of the CPA measurements, the exact process of image processing and image analysis remained a black box. In this report, we provide a detailed step-by-step instruction for CPA to quantify fibrosis in response to complex 3D biomaterials after implantation. In analogy to other CPA strategies, we segmented and analyzed the fibrotic reaction based on the occurrence of collagen fibers, as they represent the main content of fibrotic tissue.[53,61] Collagen fibers are favorable

to stain and there are several staining methods that are in use for DIA. Histochemical staining methods as well as immunohistochemical staining methods are described in the literature.[55,62-64] The histochemical staining methods mainly concentrated on Picro-Sirius Red and Masson's trichrome staining methods.[14,29,31-38,40,41,43-47,65-70] In this context, Picro-Sirius Red staining was mostly performed to evaluate organ fibrosis while Masson's trichrome stainings were commonly used to measure biomaterial-induced fibrosis. Schipke et al. assessed which staining method would be more beneficial for collagen evaluation with the help of DIA, demonstrating that both histochemical staining methods reveal equal results.[42] Based on the pathophysiological considerations of fibrosis, it is plausible that fibrotic effector cells produce a specific fibrotic microenvironment around and within a 3D macroporous scaffold. By measuring the CPA and FCT values, we quantitatively evaluated two fibrosis responses associated with foreign body reactions of 3D scaffolds in vivo: fibrotic encapsulation and fibrotic ingrowth. With respect to the quantitative measurements of these reactions, we compared the CPA analysis and FCT measurements with established semiquantitative methods for biomaterial-induced fibrosis. The quantitative fibrosis analysis methods correlated significantly with the corresponding semiquantitative scores. Thus, it could be demonstrated that DIA methods of fibrotic ingrowth and fibrotic encapsulation also conform to the conventional semiquantitative ratings and reflect the degree of fibrosis appropriately. Moreover, the CPA method will be a promising and valuable tool for the quantitative assessment of the fibrotic response against complex macroporous scaffold designs and will further our understanding of the effect of biomaterial geometry on the distribution of fibrosis responses between fibrotic encapsulation and fibrotic ingrowth. Similar to the semiquantitative evaluation, the DIA methods were able to show that the degree of the fibrotic reaction differed in between the scaffolds. Here, the pathophysiologic implications of the other processes of the foreign body reaction may play an important role. For instance, the fibrous reaction is known to be influenced by the inflammatory reaction.[1,2] In this context, the excessive capsule thickness in Scaffold E is possibly associated with a significantly stronger inflammatory reaction than the other scaffolds. However, further consideration of the foreign body reactions should not be the subject of this investigation but will be addressed in an ongoing project. With this work, the focus should be on the description of the method for quantitative evaluation strategies for fibrosis. It turned out that the CPA method is practicable, compatible with open source software and easy to learn and to manage. The measurements of the CPA values could detect even small differences in the extent of fibrotic ingrowth. One of the advantages is that the "Color Threshold" function of ImageJ can be adapted to color intensities or other colors and, thus, is theoretically compatible with several histochemical stainings. In the present study, we used Masson–Goldner's trichrome staining to stay in line with the common histopathological strategies for biomaterial-induced fibrosis. Moreover, the staining is widely available, easy to process, compatible with the slide scanner, and finally applicable for all analyses, the quantitative CPA and the FCT measurements, and the semiquantitative scorings. Our protocol is oriented by previously described procedures.[6,53,71] Nevertheless, we performed little modifications to adapt the methods on the size of our sections. For the FCT measurements, for example, we defined more locations around the surface of the implants and for the CPA analysis, we took more images than described in our references. In accordance with other reports, the images for CPA analysis were taken in 100-fold magnification to encircle a wide and representative sample area.[21,53] Despite these settings, the area per image was slightly smaller than 1 mm^2. This could depict a limitation of the method, which is based on the image tool of the used slidescanner software and unfortunately could not be extended. We further addressed the question, which DIA software would be compatible to the slide-scanner images and could also be suitable for the CPA measurements. In times of digital pathology and whole slide imaging, the market provides numerous DIA software techniques.[72] Within this diversity, we decided to use ImageJ, because it is license free and available for everyone. A disadvantage of this software was its semiautomated character. Even though we could process a whole image sequence ($N = 10$) with the threshold function at once, theoretically much larger image data sets could be processed at once. Unfortunately, imprecise markings needed manual editing to be done, yielding a semiautomated segmentation process, thus resulting in a more time-consuming process compared with the semiquantitative measurements. The authors also criticize semiautomated procedures because often the exact processes and setting calibrations are incomprehensible, which can make these methods unreliable.[42] That is why we presented the individual image processing steps in Section 2 as detailed as possible. However, so far it remains unclear whether semiautomated or fully automated strategies will be more advantageous or which software or staining method will prevail in the future evaluation of biomaterial-induced fibrosis. In relation to the actual missing diversity of fibrosis evaluation strategies for scaffold-based biomaterials, the implementation of new methods seems to be overdue. In this context, it is of special interest whether CPA analysis could range as a valuable parameter for future biocompatibility ratings. On the one hand, the method has quantitative character, produces objective data, and is therefore more accurate to detect even small differences and changes in fibrous reactions. Furthermore, it reveals additional information regarding the overall fibrotic reaction in relation to the architecture of complex 3D macroporous scaffolds. On the other hand, the collected CPA values do not account for detailed geometric and morphometric information about the fibrotic growth patterns in between the scaffolds. The transfer of this knowledge in the field of biomaterials would yield a further insight in the interactions between scaffolds and tissue interactions. This transfer would open new perspectives in our understanding of how a scaffold should be designed to influence the fibrotic growth in a desired way. In this context, future digital fibrosis analysis methods should also consider collagen polymorphism, collagen fibers directionality, and anisotropy to detect new relationships between fibrotic growth patterns and biomaterial scaffold architectures. Subsequently, an extension to 3D evaluation strategies should be taken into account, as it was already done in the fields of liver cirrhosis.[66,73,74] Finally, the present report should promote further

progress in new fibrosis evaluation strategies in the fields of TE and biomaterial research.

5 | CONCLUSION

In the present "proof-of-concept" study, we implemented the CPA method from hepatology into the field of biomaterials, and thus we quantitatively analyzed filament-based macroporous scaffolds regarding their fibrotic ingrowth reaction. The present findings revealed this fibrous reaction in a highly differentiated way. Furthermore, we quantified the fibrotic encapsulation with DIA and compared our described methods with the commonly used semiquantitative scorings. It could be demonstrated that the DIA (CPA and FCT) correlated significantly with the corresponding semiquantitative methods. In this context, CPA analysis could contribute to a more detailed understanding of the fibrous reactions on 3D scaffold-based biomaterials.

ACKNOWLEDGMENT

Open access funding enabled and organized by Projekt DEAL.

CONFLICT OF INTEREST

The authors declare no conflicts of interest.

DATA AVAILABILITY STATEMENT

The data that support the findings of this study are available from the corresponding author upon reasonable request.

REFERENCES

1. Anderson JM, Rodriguez A, Chang DT. Foreign body reaction to biomaterials. *Semin Immunol*. 2008;*20*:86-100.
2. Klopfleisch R, Jung F. The pathology of the foreign body reaction against biomaterials. *J Biomed Mater Res A*. 2017;*105*:927-940.
3. Klopfleisch R. Macrophage reaction against biomaterials in the mouse model - phenotypes, functions and markers. *Acta Biomater*. 2016;*43*:3-13. https://doi.org/10.1016/j.actbio.2016.07.003
4. Anderson JM. Future challenges in the in vitro and in vivo evaluation of biomaterial biocompatibility, Regen. *Biomaterials*. 2016;*3*:73-77.
5. Keating JH, Melidone R, Garcia-Polite F. Preclinical evaluation of mesh implants: the Pathologist's perspective. *Toxicol Pathol*. 2019;*47*:379-389.
6. Ikarashi Y, Toyoda K, Ohsawa N, et al. Comparative studies by cell culture and in vivo implantation test on the toxicity of natural rubber latex materials. *J Biomed Mater Res*. 1992;*26*:339-356.
7. Huang BJ, Hu JC, Athanasiou KA. Cell-based tissue engineering strategies used in the clinical repair of articular cartilage. *Biomaterials*. 2016;*98*:1-22.
8. Doran PM. Cartilage tissue engineering: what have we learned in practice? *Methods Mol Biol*. 2015;*1340*:3-21.
9. Vig K, Chaudhari A, Tripathi S, et al. Advances in skin regeneration using tissue engineering. *Int J Mol Sci*. 2017;*18*:789.
10. JMesquita JA, Lacerda-Santos R, Sampaio GAM, Godoy GP, Nonaka CFW, Alves PW. Evaluation in vivo of biocompatibility of differents resin-modified cements for bonding orthodontic bands. *An Acad Bras Cienc*. 2017;*89*:2433-2443.
11. Zywicka B, Szymonowicz M, Bryla D, Rybak Z. Histological evaluation of the local soft tissue reaction after implanting resorbable and non-resorbable monofilament fibers. *Polim Med*. 2016;*46*:135-143.
12. Pita PC, Pinto FC, Lira MM, Melo Fde A, Ferreira LM, Aguiar JL. Biocompatibility of the bacterial cellulose hydrogel in subcutaneous tissue of rabbits. *Acta Circul Bras*. 2015;*30*:296-300.
13. Santos RL, Moura Mde F, Carvalho FG, Guenes GM, Alves PM, Pithon MM. Histological analysis of biocompatibility of ionomer cements with an acid-base reaction. *Braz Oral Res*. 2014;*28*:1-7.
14. Graca YL, Opolski AC, Barboza BE, et al. Biocompatibility of *Ricinus communis* polymer with addition of calcium carbonate compared to titanium. Experimental study in Guinea pigs. *Rev Bras Cir Cardiovasc*. 2014;*29*:272-278.
15. Melman L, Jenkins ED, Hamilton NA, et al. Histologic and biomechanical evaluation of a novel macroporous polytetrafluoroethylene knit mesh compared to lightweight and heavyweight polypropylene mesh in a porcine model of ventral incisional hernia repair. *Hernia*. 2011;*15*:423-431.
16. Faleris JA, Hernandez RM, Wetzel D, Dodds R, Greenspan DC. In-vivo and in-vitro histological evaluation of two commercially available acellular dermal matrices. *Hernia*. 2011;*15*:147-156.
17. Sabri F, Boughter JD Jr, Gerth D, et al. Histological evaluation of the biocompatibility of polyurea crosslinked silica aerogel implants in a rat model: a pilot study. *PLoS One*. 2012;*7*:e50686.
18. Cunha SA, Rached FA, Alfredo E, Leon JE, Perez DE. Biocompatibility of sealers used in apical surgery: a histological study in rat subcutaneous tissue. *Braz Dent J*. 2011;*22*:299-305.
19. Hussein KH, Park KM, Kang KS, Woo HM. Biocompatibility evaluation of tissue-engineered decellularized scaffolds for biomedical application. *Korean J Couns Psychother*. 2016;*67*:766-778.
20. Laurinavicius A, Laurinaviciene A, Dasevicius D, et al. Digital image analysis in pathology: benefits and obligation. *Anal Cell Pathol*. 2012;*35*:75-78.
21. Pilette C, Rousselet MC, Bedossa P, et al. Histopathological evaluation of liver fibrosis: quantitative image analysis vs semi-quantitative scores. Comparison with serum markers. *J Hepatol*. 1998;*28*:439-446.
22. Masseroli M, Caballero T, O'Valle F, Del Moral RM, Perez-Milena A, Del Moral RG. Automatic quantification of liver fibrosis: design and validation of a new image analysis method: comparison with semi-quantitative indexes of fibrosis. *J Hepatol*. 2000;*32*:453-464.
23. Wright M, Thursz M, Pullen R, Thomas H, Goldin R. Quantitative versus morphological assessment of liver fibrosis: semi-quantitative scores are more robust than digital image fibrosis area estimation. *Liver Int*. 2003;*23*:28-34.
24. Hui AY, Liew CT, Go MY, et al. Quantitative assessment of fibrosis in liver biopsies from patients with chronic hepatitis B. *Liver Int*. 2004;*24*:611-618.
25. Lazzarini AL, Levine RA, Ploutz-Snyder RJ, Sanderson SO. Advances in digital quantification technique enhance discrimination between mild and advanced liver fibrosis in chronic hepatitis C. *Liver Int*. 2005;*25*:1142-1149.
26. Zaitoun AM, Al Mardini H, Awad S, Ukabam S, Makadisi S, Record CO. Quantitative assessment of fibrosis and steatosis in liver biopsies from patients with chronic hepatitis C. *J Clin Pathol*. 2001;*54*:461-465.
27. O'Brien MJ, Keating NM, Elderiny S, et al. An assessment of digital image analysis to measure fibrosis in liver biopsy specimens of patients with chronic hepatitis C. *Am J Clin Pathol*. 2000;*114*:712-718.
28. Marcos R, Braganca B, Fontes-Sousa AP. Image analysis or stereology: which to choose for quantifying fibrosis? *J Histochem Cytochem*. 2015;*63*:734-736.
29. Halasz T, Horvath G, Kiss A, et al. Evaluation of histological and non-invasive methods for the detection of liver fibrosis: the values of histological and digital morphometric analysis, liver stiffness measurement and APRI score. *Pathol Oncol Res*. 2016;*22*:1-6.

30. Pavlides M, Birks J, Fryer E, et al. Interobserver variability in histologic evaluation of liver fibrosis using categorical and quantitative scores. *Am J Clin Pathol*. 2017;*147*:364-369.
31. Calvaruso V, Burroughs AK, Standish R, et al. Computer-assisted image analysis of liver collagen: relationship to Ishak scoring and hepatic venous pressure gradien. *Hepatology*. 2009;*49*:1236-1244.
32. Hall AR, Tsochatzis E, Morris R, Burroughs AK, Dhillon AP. Sample size requirement for digital image analysis of collagen proportionate area in cirrhotic liver. *Histopathology*. 2013;*62*:421-430.
33. Hall A, Germani G, Isgro G, Burroughs AK, Dhillon AP. Fibrosis distribution in explanted cirrhotic livers. *Histopathology*. 2012;*60*:270-277.
34. Nielsen K, Clemmese JO, Vassiliadis E, Vainer B. Liver collagen in cirrhosis correlates with portal hypertension and liver dysfunction. *APMIS*. 2014;*122*:1213-1222.
35. Xu S, Wang Y, Tai DCS, et al. qFibrosis: a fully-quantitative innovative method incorporating histological features to facilitate accurate fibrosis scoring in animal model and chronic hepatitis B patients. *J Hepatol*. 2014;*61*:260-269.
36. Tsochatzis E, Bruno S, Isgro G, et al. Collagen proportionate area is superior to other histological methods for sub-classifying cirrhosis and determining prognosis. *J Hepatol*. 2014;*60*:948-954.
37. Chen SH, Peng CY, Lai HC, et al. Head-to-head comparison between collagen proportionate area and acoustic radiation force impulse elastography in liver fibrosis quantification in chronic hepatitis C. *PLoS One*. 2015;*10*:e0140554.
38. Restellini S, Goossens N, Clement S, et al. Collagen proportionate area correlates to hepatic venous pressure gradient in non-abstinent cirrhotic patients with alcoholic liver disease. *World J Hepatol*. 2018;*10*:73-81.
39. Sun Y, Zhou J, Wu X, et al. Quantitative assessment of liver fibrosis (qFibrosis) reveals precise outcomes in Ishak "stable" patients on anti-HBV therapy. *Sci Rep*. 2018;*8*:2989.
40. Vasiljevic JD, Popovic ZB, Otasevic P, et al. Myocardial fibrosis assessment by semiquantitative, point-counting and computer-based methods in patients with heart muscle disease: a comparative study. *Histopathology*. 2001;*38*:338-343.
41. Daunoravicius D, Besusparis J, Zurauskas E, et al. Quantification of myocardial fibrosis by digital image analysis and interactive stereology. *Dlagn Pathol*. 2014;*9*:114.
42. Schipke J, Brandenberger C, Rajces A, et al. Assessment of cardiac fibrosis: a morphometric method comparison for collagen quantification. *J Appl Physiol*. 2017;*122*:1019-1030.
43. Marcos-Garces V, Harvat M, Molina Aguilar P, Ferrandez Izquierdo A, Ruiz-Sauri A. Comparative measurement of collagen bundle orientation by Fourier analysis and semiquantitative evaluation: reliability and agreement in Masson's trichrome, Picrosirius red and confocal microscopy techniques. *J Microsc*. 2017;*267*:130-142.
44. Vega-Estrada A, Silvestre-Albero J, Rodriguez AE, et al. Biocompatibility and biomechanical effect of single wall carbon nanotubes implanted in the corneal stroma: a proof of concept investigation. *J Ophthalmol*. 2016;*2016*:1767.
45. Zhang WJ, Marx SK, Laue C, et al. HOE 077 reduces fibrotic overgrowth around the barium alginate microcapsules. *Transplant Proc*. 2000;*32*:206-209.
46. Zhang WJ, Laue C, Hyder A, Schrezenmeir J. Purity of alginate affects the viability and fibrotic overgrowth of encapsulated porcine islet xenografts. *Transplant Proc*. 2001;*33*:3517-3519.
47. Zhang H, Sun L, Wang W, Ma X. Quantitative analysis of fibrosis formation on the microcapsule surface with the use of picro-sirius red staining, polarized light microscopy, and digital image analysis. *J Biomed Mater Res A*. 2006;*76*:120-125.
48. Madabhushi A, Lee G. Image analysis and machine learning in digital pathology: challenges and opportunities. *Med Image Anal*. 2016;*33*:170-175. https://doi.org/10.1016/j.media.2016.06.037
49. Jenkins ED, Melman L, Deeken CR, Greco SC, Frisella MM, Matthews BD. Evaluation of fenestrated and non-fenestrated biologic grafts in a porcine model of mature ventral incisional hernia repair. *Hernia*. 2010;*14*:599-610.
50. Hadi AM, Mouchaers KT, Schalij I, et al. Rapid quantification of myocardial fibrosis: a new macro-based automated analysis. *Cell Oncol (Dordr)*. 2011;*34*:343-354.
51. Leite SN, Jordao Junio AA, Andrade TA, Masson Ddos S, Frade MA. Experimental models of malnutrition and its effect on skin trophism. *An Bras Dermatol*. 2011;*86*:681-688.
52. Caetano GF, Frade MA, Andrade TA, et al. Chitosan-alginate membranes accelerate wound healing. *J Biomed Mater Res Part B Appl Biomater*. 2015;*103*:1013-1022.
53. Caetano GF, Fronza M, Leite MN, Gomes A, Frade MA. Comparison of collagen content in skin wounds evaluated by biochemical assay and by computer-aided histomorphometric analysis. *Pharm Biol*. 2016;*54*:2555-2559.
54. DiEgidio P, Friedman HI, Gourdie RG, Riley AE, Yost MJ, Goodwin RL. Biomedical implant capsule formation: lessons learned and the road ahead. *Ann Plast Surg*. 2014;*73*:451-460.
55. Greaves NS, Iqbal SA, Hodgkinson T, et al. Skin substitute-assisted repair shows reduced dermal fibrosis in acute human wounds validated simultaneously by histology and optical coherence tomograph. *Wound Repair Regen*. 2015;*23*:483-494.
56. Thevenot P, Hu W, Tang L. Surface chemistry influences implant biocompatibility. *Curr Top Med Chem*. 2008;*8*:270-280.
57. Hogrebe NJ, Reinhardt JW, Gooch KW. Biomaterial microarchitecture: a potent regulator of individual cell behavior and multicellular organization. *J Biomed Mater Res A*. 2017;*105*:640-661.
58. Kamath S, Bhattacharyya D, Padukudru C, Timmons RB, Tang L. Surface chemistry influences implant-mediated host tissue responses. *J Biomed Mater Res Part A*. 2008;*86*:617-626.
59. Moore AL, Marshall CD, Longaker MT. Minimizing skin scarring through biomaterial design. *J Funct Biomater*. 2017;*8*:3.
60. Metcalfe AD, Ferguson MW. Bioengineering skin using mechanisms of regeneration and repair. *Biomaterials*. 2007;*28*:5100-5113.
61. Rockey DC, Bell PD, Hill JA. Fibrosis–a common pathway to organ injury and failure. *N Engl J Med*. 2015;*372*:1138-1149.
62. Qiao XH, Zhang JJ, Gao F, et al. An experimental study: quantitatively evaluating the change of the content of collagen fibres in penis with two-dimensional shear wave elastography. *Andrologia*. 2017;*49*:e12653.
63. Rogojanu R, Thalhammer T, Thiem U, et al. Quantitative image analysis of epithelial and stromal area in histological sections of colorectal cancer: an emerging Diagnostic tool. *Biomed Res Int*. 2015;*2015*:569071.
64. Calabrese G, Gulino R, Giuffrida R, et al. In vivo evaluation of biocompatibility and chondrogenic potential of a cell-free collagen-based scaffold. *Front Physiol*. 2017;*8*:984.
65. Street JM, Souza AC, Alvarez-Prats A, et al. Automated quantification of renal fibrosis with sirius red and polarization contrast microscopy. *Physiol Rep*. 2014;*2*:e12088.
66. Osman OS, Selway JL, Harikumar PE, et al. A novel method to assess collagen architecture in skin. *BMC Bioinform*. 2013;*14*:260.
67. Sun C, Wang B, Li J, et al. Quantitative measurement of breast carcinoma fibrosis for the prediction in the risk of bone metastasis. *Am J Transl Res*. 2018;*10*:1852-1859.
68. Schmidt MJ, Tschoeke A, Noronha L, et al. A histochemical analysis of collagen fibers in giant cell fibroma and inflammatory fibrous hyperplasia. *Acta Histochem*. 2016;*118*:451-455.
69. Poppler L, Cohen J, Dolen UC, et al. Histologic, molecular, and clinical evaluation of explanted breast prostheses, capsules, and acellular dermal matrices for bacteria. *Aesthet Surg J*. 2015;*35*:653-668.
70. Belladonna FG, Calasans-Maia MD, Novellino Alves AT, et al. Biocompatibility of a self-adhesive gutta-percha-based material in subcutaneous tissue of mice. *J Endod*. 2014;*40*:1869-1873.

71. Yoo JM, Ben Amara H, Kim MK, Song JD, Koo KT. Oral tissue response to soft tissue expanders prior to bone augmentation: in vitro analysis and histological study in dogs. *J Periodontal Implant Sci*. 2018;*48*:152-163.
72. Mulrane L, Rexhepaj E, Penney S, Callanan JJ, Gallagher WM. Automated image analysis in histopathology: a valuable tool in medical diagnostics. *Expert Rev Mol Diagn*. 2008;*8*:707-725.
73. Rawlins JM, Lam WL, Karoo RO, Naylor IL, Sharpe DT. Quantifying collagen type in mature burn scars: a novel approach using histology and digital image analysis. *J Burn Care Res*. 2006;*27*:60-65.
74. Altendorf H, Decenciere E, Jeulin D, et al. Imaging and 3D morphological analysis of collagen fibrils. *J Microsc*. 2012;*247*:161-175.

How to cite this article: Barsch, F., Mamilos, A., Babel, M., Wagner, W. L., Winther, H. B., Schmitt, V. H., Hierlemann, H., Teufel, A., & Brochhausen, C. (2021). Semiautomated quantification of the fibrous tissue response to complex three-dimensional filamentous scaffolds using digital image analysis. *Journal of Biomedical Materials Research Part A*, 1–12. https://doi.org/10.1002/jbm.a.37293